World Journal of
Radiology

Contents

Contents

ABOUT COVER

Editorial Board Member of *World Journal of Radiology*, Fernando Santiago, PhD, Doctor, Professor, Teacher, Department of Radiology, Santiago, FR (reprint author), Hosp Traumatol Ciudad Sanitaria Virgen de las Nie, Dept Radiol, Carretera Jaen SN, Granada 18013, Spain. ferusan12@gmail.com

AIMS AND SCOPE

The primary aim of *World Journal of Radiology* (*WJR*, *World J Radiol*) is to provide scholars and readers from various fields of radiology with a platform to publish high-quality basic and clinical research articles and communicate their research findings online.

 WJR mainly publishes articles reporting research results and findings obtained in the field of radiology and covering a wide range of topics including state of the art information on cardiopulmonary imaging, gastrointestinal imaging, genitourinary imaging, musculoskeletal imaging, neuroradiology/head and neck imaging, nuclear medicine and molecular imaging, pediatric imaging, vascular and interventional radiology, and women's imaging.

INDEXING/ABSTRACTING

The *WJR* is now abstracted and indexed in PubMed, PubMed Central, Emerging Sources Citation Index (Web of Science), Reference Citation Analysis, China National Knowledge Infrastructure, China Science and Technology Journal Database, and Superstar Journals Database. The 2022 edition of Journal Citation Reports ® cites the 2021 Journal Citation Indicator (JCI) for *WJR* as 0.48.

RESPONSIBLE EDITORS FOR THIS ISSUE

Diagnostic efficacy of diffusion-weighted imaging and semiquantitative and quantitative dynamic contrast-enhanced magnetic resonance imaging in salivary gland tumors

Erkan Gökçe, Murat Beyhan

Erkan Gökçe, Murat Beyhan, Department of Radiology, Tokat Gaziosmanpasa University, Faculty of Medicine, Tokat 60100, Turkey

Corresponding author: Erkan Gökçe, MD, Professor, Department of Radiology, Tokat Gaziosmanpasa University, Faculty of Medicine, Kaleardı Neighborhood, Muhittin Fisunoglu Street, Tokat 60100, Turkey. drerkangokce@gmail.com

Abstract

BACKGROUND

Increased use of functional magnetic resonance imaging (MRI) methods such as diffusion-weighted imaging (DWI) and dynamic contrast-enhanced (DCE) MRI consisting of sequential contrast series, allows us to obtain more information on the microstructure, cellularity, interstitial distance, and vascularity of tumors, which has increased the discrimination power for benign and malignant salivary gland tumors (SGTs). In the last few years, quantitative DCE MRI data containing T1 perfusion parameters (K_{trans}, K_{ep} and V_e), were reported to contribute to the differentiation of benign or malignant subtypes in SGTs.

AIM

To evaluate the diagnostic efficacy of DWI and semiquantitative and quantitative perfusion MRI parameters in SGTs.

METHODS

Diffusion MRI [apparent diffusion coefficient (ADC) value] with a 1.5 T MR machine, semiquantitative perfusion MRI [time intensity curve (TIC) pattern], and quantitative perfusion MRI examinations (K_{trans}, K_{ep} and V_e) of 73 tumors in 67 patients with histopathological diagnosis performed from 2017 to 2021 were retrospectively evaluated. In the ADC value and semiquantitative perfusion MRI measurements, cystic components of the tumors were not considered, and the region of interest (ROI) was manually placed through the widest axial section of the tumor. TIC patterns were divided into four groups: Type A = T_{peak} > 120 s; type B = T_{peak} ≤ 120 s, washout ratio (WR) ≥ 30%; type C = T_{peak} ≤ 120 s, WR < 30%; and type D = flat TIC. For the quantitative perfusion MRI analysis, a 3D ROI was placed in the largest solid component of the tumor, and the K_{trans}, K_{ep} and V_e values were automatically generated.

RESULTS

The majority of SGTs were located in the parotid glands (86.3%). Of all the SGTs, 68.5% were benign and 31.5% were malignant. Significant differences were found for ADC values among pleomorphic adenomas (PMAs), Warthin's tumors (WTs), and malignant tumors (MTs) ($P < 0.001$). PMAs had type A and WTs had type B TIC pattern while the vast majority of MTs and other benign tumors (OBTs) (54.5% and 45.5%, respectively) displayed type C TIC pattern. PMAs showed no washout, while the highest mean WR was observed in WTs (59% ± 11%). K_{trans} values of PMAs, WTs, OBTs, and MTs were not significantly different. K_{ep} values of PMAs and WTs were significantly different from those of OBTs and MTs. Mean V_e value of WTs was significantly different from those of PMAs, OBTs, and MTs ($P < 0.001$).

CONCLUSION

The use of quantitative DCE parameters along with diffusion MRI and semiquantitative contrast-enhanced MRI in SGTs could improve the diagnostic accuracy.

Key Words: Diffusion-weighted imaging; Dynamic contrast-enhanced imaging; Magnetic resonance imaging; Perfusion imaging; Salivary gland tumor; Tumor

Core Tip: In this study, the diagnostic features of diffusion-weighted imaging and semiquantitative and quantitative perfusion magnetic resonance imaging (MRI) parameters were evaluated in salivary gland tumors. The apparent diffusion coefficient (ADC) values of pleomorphic adenomas (PMAs) were significantly higher than those of Warthin's tumors (WTs), other benign tumors (OBTs), and malignant tumors (MTs). On semiquantitative MRI, PMAs were distinguished from all other tumors by their long T_{peak} times and lack of washout. WTs had the shortest T_{peak} and highest washout ratio values. For quantitative perfusion MRI parameters, the K_{ep} value of WTs was significantly higher than those of other tumors. The V_e values of WTs and OBTs differed significantly from those of PMAs and MTs.

INTRODUCTION

Salivary gland tumors (SGTs) account for about 2.0%-6.5% of all head and neck tumors. Approximately 70% of them originate from the parotid glands, and a small number have submandibular, sublingual, and minor salivary gland origins. While the majority of tumors from the parotid glands are benign, malignancies are more common in those located in other glands. Preoperative characterization of SGTs is important for treatment planning. The choice of surgery method for SGTs is closely associated with the histology of the tumor. Diagnosis is mostly based on combined evaluation of clinical features and findings from physical examinations, imaging and cytological observations. Fine-needle aspiration biopsy (FNAB) is the most commonly used method for cytological examinations but complex pathologies can result in false positives and false negatives in malignant tumors (MTs)[1,2]. Conventional magnetic resonance imaging (MRI) is very useful for identifying the tumor location, morphology, extension, and its association with the nerves and inner structure[1-3]. However, diagnosing MTs and benign tumors (BTs) by conventional MRI can be difficult due to overlapping findings[1,2,4]. In recent years, an increase has been reported in diagnostic accuracy in SGTs for distinguishing between MTs and BTs with the use of diffusion-weighted imaging (DWI) and dynamic contrast-enhanced (DCE) MRI techniques[1,5-9]. DCE MRI is used to track an exogenous, paramagnetic contrast agent in tissues and has been a powerful tool in the characterization of tumor hemodynamics[1,3,10,11]. As a semiquantitative method in DCE MRI, patterns have been established by measuring time to peak (T_{peak}) and washout ratio (WR) on the time intensity curve (TIC)[1,3]. T_{peak} is closely related to microvessel count while WR reflects the stromal cellularity grade. On quantitative DCE MRI, on the other hand, perfusion parameters such as K_{trans} [volume transfer constant between blood plasma and the extracellular extravascular space (EES)], K_{ep} (flux rate constant between the EES and plasma), and V_e (EES fractional volume) are used[1,3]. Although there are many studies dealing with diffusion and semiquantitative

DCE MRIs in SGTs, the number of quantitative MRI studies is limited[12-15]. In the present study, the diagnostic value of diffusion MRI and semiquantitative and quantitative perfusion MRI parameters was evaluated in SGTs.

MATERIALS AND METHODS

Patients

The study was conducted retrospectively following approval by the local ethics committee (20-KAEK-105). A total of 67 patients with tumors originating from or involving the salivary glands were included. The study included patients who had swelling of the face or in the salivary glands, who were subjected to MRI, diffusion MRI, and perfusion MRI examinations at our hospital between April 2017 and February 2021 and who were diagnosed histopathologically after FNAB, Tru-cut biopsy, or surgical removal. For this study, patients whose neck and maxillofacial MRI examination reports included the description of a mass in the salivary glands were surveyed in picture archiving and communication systems. A total of 33 patients were excluded: 2 patients with intra-lesion hemorrhage due to FNAB before the MRI examination, 16 patients who had contrast-enhanced MRI but did not have perfusion MRI series, and 15 patients whose diagnosis was not confirmed histopathologically. Thus, a total of 73 MTs and BTs, which originated from major and minor salivary glands in 67 patients, were included in the study (Figure 1).

MRI scanning and measurements

MRI was performed on a 1.5 T superconducting MRI system [General Electric (GE) Signa Explorer Software Version 25; GE Healthcare, Milwaukee, WI, United States, 2016] with head and neck array coils. Routine MRI sequences included axial T1-weighted [time to repetition/time to echo (TR/TE), 456 ms/8.1 ms], in phase axial T2-weighted (TR/TE, 3711 ms/82.8 ms), sagittal T2-weighted (TR/TE, 4499 ms/88.2 ms), and coronal T2-weighted (TR/TE, 4380 ms/84.6 ms). DCE MRI was performed with a T1-weighted 3D fast spoiled gradient echo sequence [TR/TE/time to inversion, 3.8 ms/1.3 ms/15 ms; flip angle, 20°]. The contrast agent Gd-DTPA (Dotarem, Guerbet, France) was injected after the fourth dynamic sequence acquisition at a rate of 2.0 mL/s *via* the right antecubital vein. The contrast agent was administered at a dose of 0.2 mmoL/kg body weight. Immediately after the injection of the contrast agent, a 20 mL saline flush was carried out at the same injection rate. In total, 18-21 dynamic sequence acquisitions with 30 dynamic images per sequence were performed with total scanning time ranging from 3 min and 11 s to 5 min and 24 s. The location, morphology, and internal structure of the tumor were evaluated by conventional MRI (Figures 2A and B, 3A and B, 4A and B, 5A and B).

DWI was performed using a multislice echo-planar single-shot spin-echo sequence, on the axial plane (TR/TE = 5476 ms/95.4 ms, field of view = 26 cm, matrix = 96 × 128, section thickness = 4-5 mm, and interslice gap = 4 mm). Three diffusion gradients were applied sequentially in the x, y, and z directions with *b* values of 0 and 1000 s/mm^2 (Figure 2B). The acquisition time varied from 60 s to 120 s. The apparent diffusion coefficient (ADC) maps were generated automatically.

"GE Advantage Windows Workstation 4.7" was used to determine ADC values on diffusion MRI and to perform measurements in semiquantitative and quantitative perfusion MRI. Image analysis and region of interest (ROI) measurements were carried out on a consensus basis by two neuroradiologists (Erkan Gökçe and Murat Beyhan with more than 12 and 7 years of work experience, respectively) who were not aware of the clinical status of the patients. On ADC value measurements, cystic components of the tumors were not considered, the ROI was manually placed through the widest axial section of the tumor, and the ADC value was determined as mm^2/s (Figures 2C, 3C, 4C and 5C). Semiquantitative analysis of DCE MRI was based on TIC (Figures 2D and E, 3D and E, 4D and E, 5D and E). T_{peak} was measured as the time from the point where the lesion began to show contrast enhancement to the point with the highest level of contrast enhancement. TICs were evaluated in four different categories based on Yabuuchi *et al*[10]: Type A = T_{peak} > 120 s; type B = T_{peak} ≤ 120 s, WR ≥ 30%; type C = T_{peak} ≤ 120 s, WR < 30%; and type D = flat TIC. To confirm the accuracy of TIC and perfusion biomarker analyses, ROIs were drawn in a way to avoid the vascular and cystic parts of the tumors. Quantitative perfusion DCE MRI parameters were measured using the Tofts kinetic model[16]. For quantitative perfusion MRI analysis, a 3D ROI was placed in the largest solid component of the tumor, and the K_{trans}, K_{ep} and V_e values were generated automatically (Figures 2F-H, 3F-H, 4F-H, 5F-H).

Statistical analysis

Statistical analyses were performed using SPSS 18.0 software (IBM, Chicago, IL, United States) and MedCalc statistical software version 20.009 (MedCalc software bvba, Ostend, Belgium). For each parameter, the conformity of the groups to the normal distribution was evaluated by the Shapiro-Wilk test, and the Levene test was used to evaluate the homogeneity of variances. Data are expressed as the mean ± SD or frequency and percent. One-way ANOVA was used for the groups with a normal distribution for comparison of the groups, and Bonferroni correction was applied in multiple comparisons. The Kruskal-Wallis test was used to compare the groups that did not fit the normal distribution, and
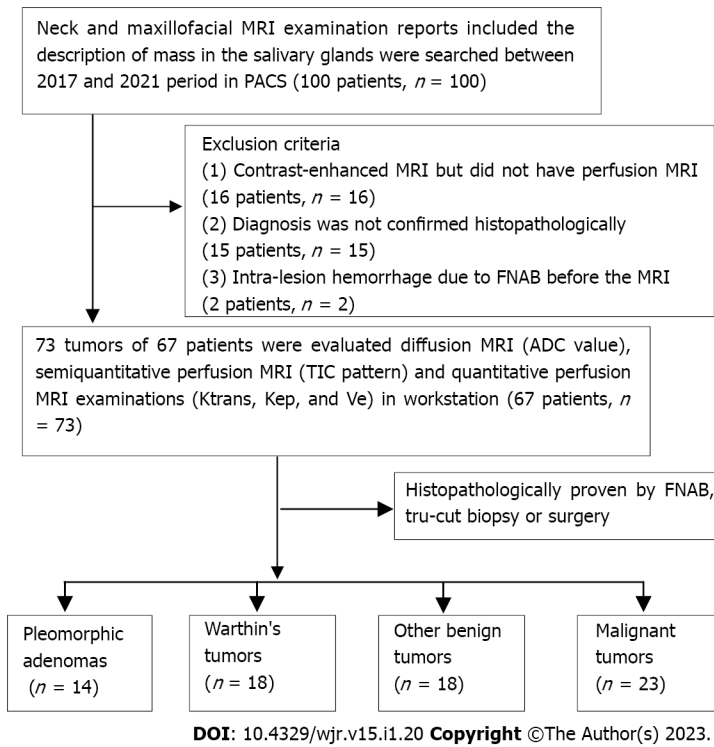
Figure 1 Patient inclusion and exclusion flowchart.
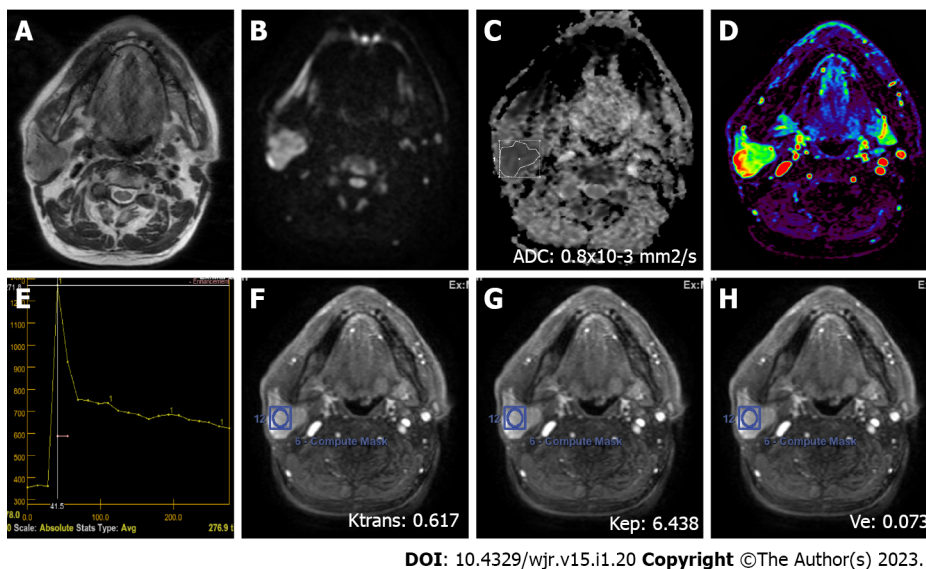
Figure 2 A 72-year-old male patient with a Warthin's tumor in the right parotid gland. A: On axial plane T2-weighted image, a mildly hypointense (compared to the gland), smooth-contoured mass localized in the center of the parotid gland is observed; B: On the diffusion-weighted image, the mass appears to be hyperintense; C: ADC value was 0.8×10^{-3} mm^2/s on the apparent diffusion coefficient map; D: The mass is hyperperfused on color-coded perfusion image; E: Type B time intensity curve shows a washout ratio of 75%; F, G, and H: K$_{trans}$, K$_{ep}$, and V$_e$ values on quantitative perfusion images were 0.617 min^{-1}, 6.438 min^{-1}, and 0.073, respectively. ADC: Apparent diffusion coefficient.

Bonferroni correction was applied in multiple comparisons. The area under curve (AUC), sensitivity, specificity, positive predictive value (PPV), negative predictive value (NPV), and cut-off values of diagnostic parameters were calculated for each tumor group by performing receiver operating characteristic curve (ROC) analysis.
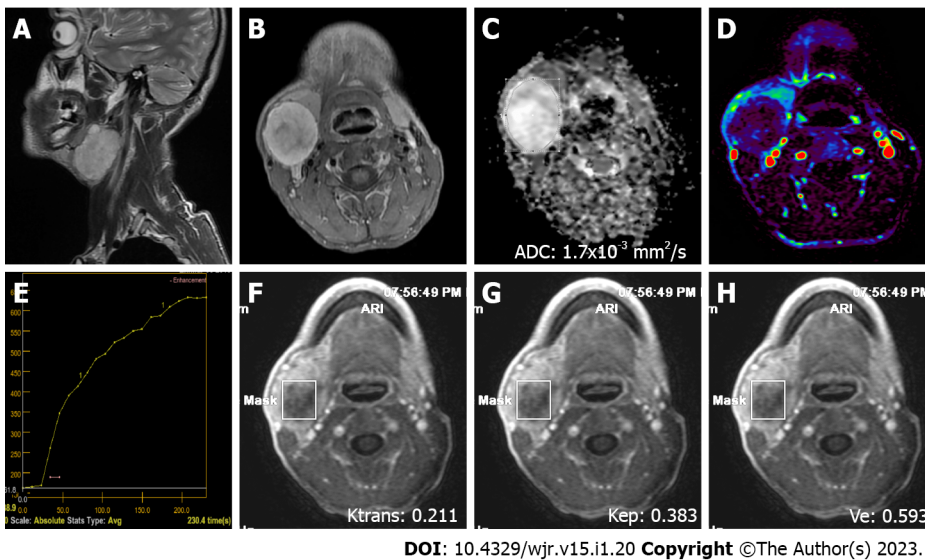
**Figure 3 A 38-year-old male patient with a pleomorphic adenoma in the right submandibular gland.** A: On sagittal plane T2-weighted image, a hyperintense (compared to the gland), smooth, slightly lobule-contoured mass is observed; B: On contrast-enhanced axial plane T1-weighted image, intense contrast-enhancement is observed in the mass; C: The mass is hyperintense on the apparent diffusion coefficient map due to facilitated diffusion (ADC value: 1.7×10^{-3} mm^2/s); D: The mass is hypoperfused on color coded perfusion image; E: The tumor has type A time intensity curve; F, G, and H: K_{trans}, K_{ep}, and V_e values on quantitative perfusion images were 0.211 min^{-1}, 0.383 min^{-1}, and 0.593, respectively. ADC: Apparent diffusion coefficient.
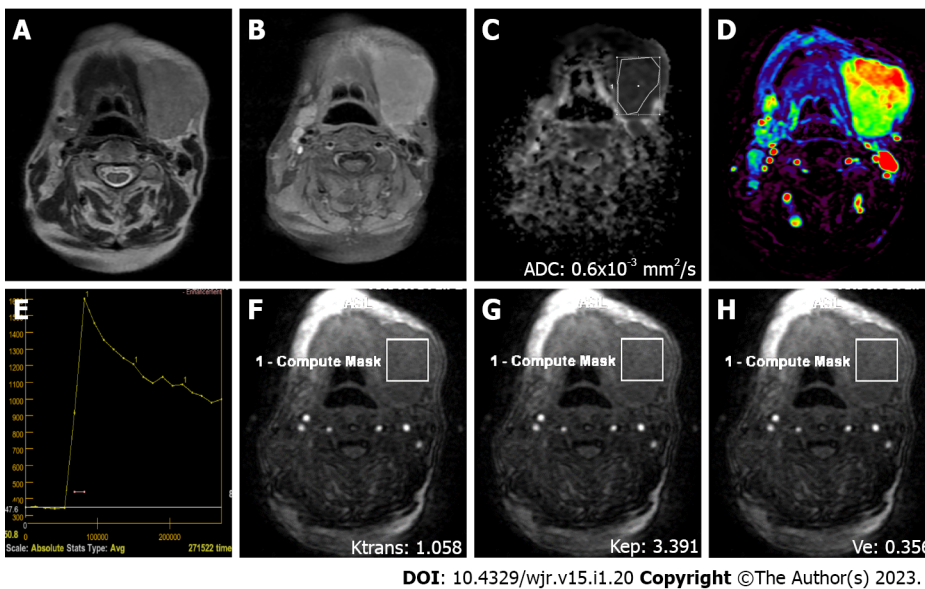
Figure 4 A 76-year-old female patient with diffuse large B cell lymphoma and a mass in the left submandibular gland region. A: On axial T2-weighted image, a smooth-contoured mass with homogeneous internal structure and an intensity similar to that of the submandibular gland is observed; B: Axial contrast-enhanced image shows the intense homogeneous contrast enhancement of the mass; C: On the apparent coefficient mapping image, the mass features prominent diffusion restriction (ADC value: 0.6×10^{-3} mm^2/s); D: The mass is hyperperfused on color coded perfusion image; E: Type B time intensity curve shows a 48% washout ratio; F, G, and H: K_{trans}, K_{ep}, and V_e values on quantitative perfusion images were 1.058 min^{-1}, 3.391 min^{-1}, and 0.356, respectively. ADC: Apparent diffusion coefficient.

RESULTS

The age range of the 67 patients (40 male and 27 female) included in the study was 12-93 years (mean age = 56.9 ± 15.8 years). One patient had three lesions in the salivary glands, while four patients had two and the remaining 62 had one lesion. Thus, 73 lesions in 67 patients were evaluated. The majority of the lesions (86.3%) were located in the parotid glands, while a small number (4.1%) originated from minor salivary glands. The locations, numbers, and frequencies of SGTs are shown in Table 1. Approximately two-thirds of the lesions (68.5%) were benign (Figures 2 and 3), and one-third (31.5%) was malignant (Figures 4 and 5). Warthin's tumors (WTs) (36.0%) were the most common BTs, followed by pleomorphic adenomas (PMAs) (28.0%). Of the MTs, squamous cell cancer (47.8%), adenoid cystic

Table 1 Locations, numbers, and frequencies of salivary gland tumors	
Location	*n (%)*
Unilateral parotid gland	61 (83.6)
Submandibular gland	6 (8.2)
Minor salivary gland	3 (4.1)
Bilateral parotid gland	2 (2.7)
Sublingual gland	1 (1.4)

n: Number of salivary gland tumors
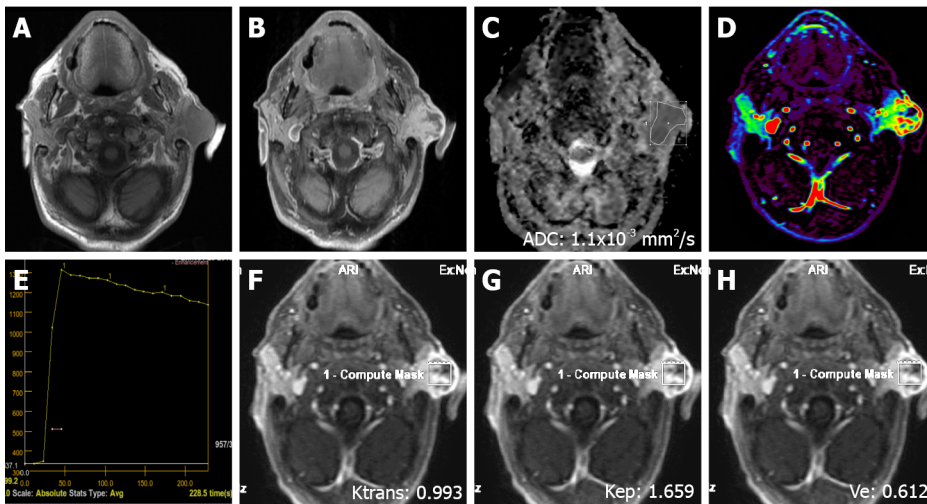
DOI: 10.4329/wjr.v15.i1.20 **Copyright** ©The Author(s) 2023.

Figure 5 A 79-year-old male patient with squamous cell cancer in the left parotid gland. A: On axial plane T1-weighted image, an irregularly contoured, hypointense mass involving skin and subcutaneous tissues is observed; B: On axial contrast-enhanced T1-weighted image, the mass shows an intense heterogeneous contrast enhancement; C: ADC value on the apparent diffusion coefficient map was 1.1×10^{-3} mm^2/s; D: The mass is heterogeneously hyperperfused on color coded perfusion image; E: Type C time intensity curve shows a 10% washout ratio; F, G, and H: K_{trans}, K_{ep}, and V_e values on quantitative perfusion images were 0.993 min^{-1}, 1.659 min^{-1}, and 0.612, respectively. ADC: Apparent diffusion coefficient.

cancers (13.0%), and malignant lymphomas (13.0%) were the most common. The numbers of benign and malignant SGTs are provided in Table 2. The ADC values of PMAs were significantly higher than those of WTs, other benign tumors (OBTs), and MTs ($P < 0.001$). However, there was no significant difference in ADC values for OBTs, WTs, and MTs. Significant differences were not found for ADC values of all BTs and MTs. The mean ADC values of SGTs are shown in Table 3.

An evaluation of T_{peak} values of semiquantitative perfusion MRI parameters revealed that PMAs reached T_{peak} significantly later (mean $T_{peak} = 202.74 \pm 21.48$ s) than WTs, OBTs, and MTs while the difference between OBTs and MTs for T_{peak} values was not significant. WTs reached T_{peak} significantly earlier than other tumors. With regard to WR, no washout was observed in PMAs. WTs had the highest mean WR value (59% ± 11%), which was significantly different from the mean WR values of MTs and OBTs. PMAs had type A and WTs had type B TIC pattern, while the majority of MTs and OBTs (54.5% and 45.5%, respectively) exhibited type C TIC pattern. Semiquantitative DCE MRI parameters of SGTs are provided in Table 4.

For quantitative perfusion MRI parameters, K_{trans} values of PMAs, WTs, OBTs, and MTs were not significantly different. The K_{ep} value of WTs, on the other hand, was significantly higher than those of other tumors ($P < 0.001$). For V_e value, WTs and OBTs differed significantly from PMAs and MTs ($P < 0.001$). An evaluation of all BTs and MTs showed significant differences for K_{ep} and V_e values ($P < 0.05$) but not for K_{trans} values. Quantitative DCE MRI parameters of SGTs are shown in Table 3.

The results of ROC analysis and cut-off values used for the parameters of DWI, semiquantitative and quantitative MRI of PMAs, WTs, and malignant SGTs are given in Table 5.

Table 2 Numbers of benign and malignant salivary gland tumors

Benign SGTs	*n* (%)	Malignant SGTs	*n* (%)
Warthin's tumor	18 (24.7)	Squamous cell carcinoma	11 (15.1)
Pleomorphic adenoma	14 (19.2)	Adenoid cystic carcinoma	3 (4.1)
Inflammatory process	12 (16.4)	Malignant lymphoma	3 (4.1)
Lipoma	4 (5.5)	Adenocarcinoma	1 (1.4)
Benign cystic lesions	1 (1.4)	Mucoepidermoid carcinoma	1 (1.4)
		Carcinoma ex pleomorphic adenoma	1 (1.4)
Other benign lesions	1 (1.4)	Acinic cell carcinoma	1 (1.4)
		Follicular dendritic cell sarcoma	1 (1.4)
		Salivary duct carcinoma	1 (1.4)
Total	50 (68.5)		23 (31.5)

SGTs: Salivary gland tumors; *n*: Number of salivary gland tumors

Table 3 Mean ADC values and quantitative dynamic contrast-enhanced magnetic resonance imaging parameters of different histopathologic salivary gland tumors

	Pleomorphic adenoma	Warthin's tumor	Other benign tumors	Malignant tumors	*P* value
ADC ($\times 10^{-3}$ mm²/s)	1.61 ± 0.26 (a)	0.72 ± 0.09 (b)	0.77 ± 0.19 (b)	0.96 ± 0.33 (b)	< 0.001
K_{trans} (min⁻¹)	0.42 ± 0.35	0.75 ± 0.55	0.57 ± 0.37	0.77 ± 0.56	0.131
K_{ep} (min⁻¹)	0.69 ± 0.33 (a)	6.2 ± 3.13 (b)	1.95 ± 0.94 (c)	1.72 ± 0.92 (c)	< 0.001
V_e	0.65 ± 0.25 (a)	0.11 ± 0.04 (b)	0.3 ± 0.12 (c)	0.48 ± 0.24 (ac)	< 0.001

Data are shown as the mean ± SD. One-way ANOVA was used. abc: Indicates that means with the same letters in the same column are not significantly different; $P < 0.05$ indicates a statistically significant difference among the groups. ADC: Apparent diffusion coefficient; K_{trans}: Volume transfer constant between blood plasma and the extracellular extravascular space; K_{ep}: Flux rate constant between the EES and plasma; V_e: EES fractional volume; EES: Extracellular extravascular space.

Table 4 Semiquantitative dynamic contrast-enhanced magnetic resonance imaging parameters of different histopathologic salivary gland tumors

	TIC Pattern, *n*(%)				T_{peak} (s)	WR (%)
	A	B	C	D		
Pleomorphic adenomas	14 (70.0)	0 (0)	0 (0)	0 (0)	202.74 ± 21.48 (a)	-
Warthin's tumors	0 (0)	18 (66.7)	0 (0)	0 (0)	20.26 ± 11.72 (b)	59.33 ± 10.99 (a)
Other benign tumors	4 (20.0)	4 (14.8)	10 (45.5)	0 (0)	74.94 ± 75.47 (c)	17.89 ± 14.99 (b)
Malignant tumors	2 (10.0)	5 (18.5)	12 (54.5)	4 (100)	60.60 ± 55.78 (c)	18.48 ± 18.38 (b)
P value	< 0.001				< 0.001	< 0.001

Data are shown as the mean ± SD. One-way ANOVA was used. abc: Indicates that the means with the same letters in the same column are not significantly different. TIC: Time intensity curve; T_{peak}: Time to peak; WR: Washout ratio; *n*: Number of salivary gland tumors.

DISCUSSION

In recent years, diffusion MRI has been an essential complement to conventional sequences in the radiological evaluation of SGTs[1,3,6-10,13-15,17,18]. Diffusion MRI allows us to evaluate the cellularity in tissues and the changes that physiological processes create on microstructural features. As malignant or benign SGTs include a highly heterogeneous group, their ADC values could also be highly variable. In cell-rich tumors such as WT and lymphoma, ADC values are low, but tumors containing hetero-

Table 5 Comparison of pleomorphic adenomas, Warthin's tumors, and malignant salivary gland tumors by ROC analysis using ADC, T_{peak}, K_{trans}, K_{ep}, and V_e values

Variable	Cut-off	AUC (95% CI)	Sensitivity	Specificity	PPV	NPV	*P* value
Pleomorphic adenomas							
ADC value	> 1.1	0.977 (0.911-0.998)	1.000	0.898	0.700	1.000	< 0.001
T_{peak}	> 120	0.947 (0.868-0.986)	1.000	0.898	0.700	1.000	< 0.001
K_{trans}	≤ 0.46	0.702 (0.584-0.804)	0.857	0.627	0.353	0.949	0.005
K_{ep}	≤ 1.14	0.926 (0.840-0.974)	0.929	0.831	0.565	0.980	< 0.001
V_e	≥ 0.4	0.849 (0.746-0.922)	0.929	0.729	0.448	0.977	< 0.001
Warthin's tumors							
ADC value	≤ 0.8	0.742 (0.626-0.837)	0.944	0.582	0.425	0.970	< 0.001
T_{peak}	≤ 19.1	0.869 (0.769-0.936)	0.667	0.909	0.706	0.893	< 0.001
WR	> 43	0.981 (0.917-0.999)	0.944	0.909	0.773	0.980	< 0.001
K_{trans}	> 0.3	0.577 (0.455-0.692)	0.889	0.346	0.308	0.905	0.291
K_{ep}	> 2.44	0.973 (0.905-0.997)	1.000	0.855	0.692	1.000	< 0.001
V_e	≤ 0.17	0.958 (0.883-0.991)	1.000	0.909	0.783	1.000	< 0.001
Malignant tumors							
ADC value	> 0.7	0.541 (0.420-0.658)	0.783	0.440	0.391	0.815	0.569
T_{peak}	≤ 120	0.531 (0.410-0.649)	0.913	0.360	0.396	0.900	0.648
WR	≤ 49	0.562 (0.441-0.678)	1.000	0.300	0.397	1.000	0.351
K_{trans}	> 0.53	0.599 (0.477-0.712)	0.652	0.600	0.429	0.789	0.194
K_{ep}	≤ 3.7	0.592 (0.471-0.706)	1.000	0.300	0.397	1.000	0.160
V_e	> 0.35	0.702 (0.584-0.804)	0.696	0.660	0.485	0.825	0.001

ADC ($\times 10^{-3}$ mm²/s): Apparent diffusion coefficient; T_{peak} (s): Time to peak; K_{trans} (min⁻¹): Volume transfer constant between blood plasma and the extracellular extravascular space; K_{ep} (min⁻¹): Flux rate constant between the EES and plasma; V_e: EES fractional volume; AUC: Area under the ROC curve; CI: Confidence interval; PPV: Positive predictive value; NPV: Negative predictive value; WR (%): Washout ratio; EES: Extracellular extravascular space.

geneous components such as PMA have higher ADC values[1,13]. In many DWI studies involving SGTs, ADC values were reported to be useful in distinguishing BTs and MTs[6-8,17,19-21]. However, there are also studies reporting that DWI was not sufficient to make this distinction but ADC values could be useful in distinguishing some subtypes of MTs or BTs[10,22-24]. An evaluation of mean ADC values of all BTs and MTs in the present study showed that ADC values of BTs ($0.98 \times 10^{-3} \pm 0.43$ mm²/s) and MTs ($0.95 \times 10^{-3} \pm 0.31$ mm²/s) were similar and did not differ significantly. However, when specific tumoral subgroups were evaluated, significant differences were found in the mean ADC values among PMAs, WTs, and MTs ($P < 0.001$). In a ROC analysis using an ADC cut-off value of $> 1.1 \times 10^{-3}$ mm²/s for PMAs, the AUC, sensitivity, and specificity were 97.7%, 100%, and 89.8%, respectively. A ROC analysis of WTs using an ADC cut-off value of $\leq 0.8 \times 10^{-3}$ mm²/s, on the other hand, resulted in AUC, sensitivity, and specificity values of 74.2%, 94.4%, and 58.2%, respectively. These values were 54.1%, 78.3%, and 44.0%, respectively, for MTs with an ADC cut-off value of $> 0.7 \times 10^{-3}$ mm²/s. In the present study, the mean ADC value of malignant lymphomas was $0.56 \times 10^{-3} \pm 0.05$ mm²/s, which was well below the average ADC value of all MTs. This finding indicated that diffusion MRI could be more useful in distinguishing the subgroups within both BTs and MTs than contributing to a more general distinction between MTs and BTs.

In addition to diffusion MRI, the parameters of semiquantitative DCE MRI (TIC patterns) have also been frequently used in recent years for the differential diagnosis of SGTs[9,12,20,25,26]. On DCE MRI, TIC is obtained from signal intensity changes before the contrast agent administration, during the transition of contrast agent from the capillary bed to extravascular-intercellular distance, and during the washing of contrast agent from the tissue[1,18]. TIC patterns are correlated with tumor cellularity and vascularity[1,5,18,27]. PMAs have progressive contrast-enhancement due to low microvessel count and cellularity-stromal grade, and their washout patterns are mostly negative and, to a lesser degree, in the form of a plateau[1,27]. In the present study, type A TIC pattern (curve pattern with progression towards the late phases) was observed in all PMAs. T_{peak} values ranged from 161.80 s to 251.70 s. The

average T_{peak} value of PMAs (202.74 ± 21.48 s) was significantly longer compared to the T_{peak} values of all other SGTs. In ROC analysis of PMAs using a cut-off value of T_{peak} > 120 s, AUC, sensitivity, specificity, PPV, and NPV were 94.7%, 100%, 89.8%, 70.0%, and 100%, respectively. WTs feature rapid contrast enhancement and washout due to their high microvessel count and cellularity-stromal grade. In the present study, type B TIC pattern (T_{peak} ≤ 120 s, WR ≥ 30%) was observed in all WTs. T_{peak} values ranged from 10.80 s to 46.40 s, while WR varied from 31% to 75%. The mean T_{peak} of WTs (20.26 ± 11.72 s) was significantly shorter than that of other parotid lesions. The average WR value of WTs (59.33% ± 10.99%) was significantly higher than that of any other tumors. In ROC analysis of WTs using a cut-off value of WR > 43%, AUC, specificity, and PPV were quite high (98.1%, 94.4%, and 90.9%, respectively). Due to their high microvessel count and lower cellularity-stromal grade, MTs have rapid enhancement but their washouts tend to be slower than those of WTs[1,27]. In the present study, the mean T_{peak} value of MTs (60.60 ± 55.78 s) was significantly shorter than the T_{peak} value of PMAs. The mean WR value of MTs (18.48 ± 18.38%) was significantly lower than that of WTs, but was not different from the mean WR value of OBTs. In ROC analysis of MTs with cut-off values of T_{peak} ≤ 120 s and WR ≤ 49%, sensitivities were quite high (91.3% and 100%, respectively) but specificities were quite low (36.0% and 30.0%, respectively). A survey of semiquantitative DCE MRI studies in the literature showed that PMAs generally had type A pattern, while WTs had type B and MTs had type C TIC patterns[4,5,26]. TIC patterns are considered to have a higher diagnostic accuracy in distinguishing subgroups in SGTs compared to their power to distinguish all BTs from MTs. However, it was mentioned that TIC patterns had higher specificity especially in PMAs and WTs while their specificity in MTs was lower[4,18,25,26]. In their study with all SGTs, Lam *et al*[26] showed that all MTs except lymphomas showed type C TIC pattern (T_{peak} < 150 s and WR < 30%), while 70% of lymphomas had type B TIC pattern (T_{peak} < 150 s and WR ≥ 30%). Similar to the findings of Lam *et al*[26], 66.7% of lymphomas in the present study showed type B TIC pattern. However, unlike their findings, some other MTs showed types A, B, and D TIC patterns. There are also studies in the literature reporting that all WTs had type B TIC pattern[4,10,12]. In accordance with their findings, 100% of WTs in the present study featured type B TIC pattern. Subtypes of SGTs in the present study generally had similar TIC patterns to those reported in the literature.

The literature contains several studies on quantitative DCE perfusion MRI parameters (K_{trans}, K_{ep}, and V_e) in SGTs[3,14,15,28]. In these studies, mean K_{trans} values for PMAs ranged from 0.101 ± 0.069 min^{-1} to 0.217 ± 0.036 min^{-1}, mean K_{ep} values from 0.245 ± 0.160 min^{-1} to 0.567 ± 0.048 min^{-1}, and mean V_e values from 0.360 to 0.590 ± 0.478, while mean K_{trans} values for WTs varied between 0.105 min^{-1} ± 0.064 min^{-1} and 0.464 ± 0.036 min^{-1}, mean K_{ep} values between 0.729 ± 0.112 min^{-1} and 2.299 ± 1.312 min^{-1}, and mean V_e values between 0.1439 ± 0.093 and 0.272 ± 0.013. For MTs, mean K_{trans} values varied from 0.130 ± 0.035 min^{-1} to 0.327 ± 0.030 min^{-1}; mean K_{ep} values from 0.463 ± 0.103 min^{-1} to 0.784 ± 0.064 min^{-1}; and mean V_e values from 0.264 ± 0.119 to 0.445 ± 0.025. In all of these studies in the literature, the K_{trans} values of PMAs were lower than those of other SGTs[3,14,15,28]. Xu *et al*[3] found that the mean K_{trans} value of PMAs was slightly different from that of WTs (P = 0.05). Yabuuchi *et al*[14] found no significant differences among K_{trans} values of other SGTs. Huang *et al*[15] found that the K_{trans} values of PMAs were significantly lower than those of other SGTs. Similar to the results of Yabuuchi *et al*[14], in our study, mean K_{trans} value of PMAs was the lowest among all SGTs, but it was not significantly different from those of other tumors. In the studies by Xu *et al*[3], Yabuuchi *et al*[14], and Huang *et al*[15], the mean K_{ep} value was the lowest in PMAs and highest in WTs. K_{ep} values of PMAs, WTs, and MTs in the studies of both Xu *et al*[3] and Yabuuchi *et al*[14] were significantly different. However, in the study by Huang *et al* [15], the K_{ep} value of only WTs was significantly different from those of other tumors. In another study by Huang *et al*[28], significant differences were found in K_{ep} values between WTs and PMAs, and between WTs and OBTs. Similar to the results of those studies in the literature, the mean K_{ep} value in the present study was the lowest in PMAs and highest in WTs, and K_{ep} values of PMAs and WTs were significantly different from those of other tumors[3,13,14,28]. Xu *et al*[3], Yabuuchi *et al*[14], and Huang *et al*[15] found that mean V_e values of WTs were significantly lower than those of other tumors. Similar to the results of their studies, the mean V_e value of WTs in the present study was significantly lower than those of other tumors[3,14]. In another study by Huang *et al*[28], unlike other studies, the V_e value of WTs and the V_e values of PMAs and OBTs were found to be significantly lower. In ROC analysis using a cut-off value of K_{ep} ≥ 2.44 min^{-1} for WTs, the AUC, sensitivity, and specificity were 97.3%, 100%, and 85.5%, respectively. On the other hand, in ROC analysis using a cut-off value of V_e ≤ 0.17, quite high AUC, sensitivity, and specificity values (95.8%, 100%, and 90.9%, respectively) were obtained. High K_{ep} and low V_e values in WTs are explained by the limited extravascular and extracellular space in these tumors. As many studies in the literature and the present study revealed, ADC and TIC patterns of WTs could overlap with those of MTs[11]. However, similar to the findings of the studies in the literature, the present study showed that quantitative perfusion MRI parameters K_{ep} and V_e could contribute greatly to distinguishing WTs from MTs[3,14,15]. Nevertheless, our findings need to be verified by future quantitative perfusion MRI studies performed with larger series.

There are some limitations in this study. First, the parameters (number of dynamic series, acquisition time, *etc.*) varied on perfusion MRI series due to the retrospective nature of the study. Second, most of the tumors in our study were benign SGTs, and the number of MTs in the primary salivary gland was relatively low, which may have resulted in an overestimation of the diagnostic accuracy. Third, the

manual definition of ROI might have increased the variability in quantitative measurements. Although the cystic-necrotic components of the lesions were excluded from the ROI in our study, contamination of these areas can lead to significant changes in quantitative values, even if it is small in manual measurements. Fourth, for the measurements of ADC values and semiquantitative and quantitative DCE perfusion MRI parameters, interobserver agreement could not be evaluated in the study as the measurements were made by two observers with consensus.

CONCLUSION

Combined use of quantitative DCE MRI along with diffusion MRI and semiquantitative DCE MRI could help radiologists in the differential diagnosis of different subtypes of SGTs by providing higher diagnostic accuracy.

ARTICLE HIGHLIGHTS

Research background

Conventional magnetic resonance imaging (MRI) provides more data than other radiological modalities in determining the extent of tumor spread in salivary gland tumors (SGTs) and assessing its relationship to vascular and neural structures, but falls short of distinguishing subtypes of SGTs. As the malignant or benign nature of SGTs affects the treatment protocol, it is important to differentiate between malignant (MTs) and benign tumors (BTs) noninvasively with high diagnostic accuracy.

Research motivation

In recent years, advanced MRI techniques such as diffusion-weighted imaging (DWI) and semi-quantitative MRI have been increasingly used in the radiological evaluation of SGTs. However, various studies on quantitative dynamic contrast-enhanced (DCE) perfusion MRI parameters (K_{trans}, K_{ep}, and V_e) in SGTs are limited. Therefore, in this study, the effectiveness of advanced MRI applications, including all three methods, in the diagnosis of SGTs was evaluated in light of the literature.

Research objectives

To determine the diagnostic efficiency of DWI and DCE (semiquantitative perfusion) MRI and quantitative perfusion MRI parameters in SGTs.

Research methods

Apparent diffusion coefficient (ADC) values of SGTs on DWI were measured with manually inserted regions of interest, excluding the cystic components of the tumors. Time intensity curve (TIC) patterns were created for semiquantitative perfusion MRI based on T_{peak} and washout ratios (WRs) of tumors. On quantitative DCE MRI, perfusion parameters such as K_{trans} [volume transfer constant between blood plasma and extracellular extravascular space (EES)], K_{ep} (flux rate constant between the EES and plasma), and V_e (EES fractional volume) were used.

Research results

The ADC values of pleomorphic adenomas (PMAs) were significantly higher than those of Warthin's tumors (WTs), other benign tumors (OBTs), and MTs ($P < 0.001$). However, there was no significant difference in ADC values for OBTs, WTs, and MTs. PMAs had type A and WTs had type B TIC pattern while the vast majority of MTs and OBTs (54.5% and 45.5%, respectively) displayed type C TIC pattern. PMAs showed no washout, while the highest mean WR was observed in WTs. For quantitative perfusion MRI parameters, the K_{ep} value of WTs was significantly higher than those of other tumors ($P < 0.001$). For the V_e value, WTs and OBTs differed significantly from PMAs and MTs ($P < 0.001$). K_{trans} values of PMAs, WTs, OBTs, and MTs were not significantly different.

Research conclusions

DWI and semiquantitative and quantitative perfusion MRI, which provide more information on the microstructure, cellularity, interstitial distance, and vascularity of tumors, have increased the discrimination power for subtypes of SGTs.

Research perspectives

Although there is some overlap in the findings of the subtypes of SGTs obtained by advanced MRI methods, the combined use of DWI and semiquantitative and quantitative perfusion MRI will increase the power for distinguishing subtypes of SGTs.

ACKNOWLEDGEMENTS

FOOTNOTES

ORCID number: Erkan Gökçe 0000-0003-3947-2972; Murat Beyhan 0000-0002-8630-4632.

REFERENCES

1   **Gökçe E**. Multiparametric Magnetic Resonance Imaging for the Diagnosis and Differential Diagnosis of Parotid Gland Tumors. *J Magn Reson Imaging* 2020; **52**: 11-32 [PMID: 32065489 DOI: 10.1002/jmri.27061]

2   **Lobo R**, Hawk J, Srinivasan A. A Review of Salivary Gland Malignancies: Common Histologic Types, Anatomic Considerations, and Imaging Strategies. *Neuroimaging Clin N Am* 2018; **28**: 171-182 [PMID: 29622112 DOI: 10.1016/j.nic.2018.01.011]

3   **Xu Z**, Zheng S, Pan A, Cheng X, Gao M. A multiparametric analysis based on DCE-MRI to improve the accuracy of parotid tumor discrimination. *Eur J Nucl Med Mol Imaging* 2019; **46**: 2228-2234 [PMID: 31372671 DOI: 10.1007/s00259-019-04447-9]

4   **Zheng N**, Li R, Liu W, Shao S, Jiang S. The diagnostic value of combining conventional, diffusion-weighted imaging and dynamic contrast-enhanced MRI for salivary gland tumors. *Br J Radiol* 2018; **91**: 20170707 [PMID: 29902075 DOI: 10.1259/bjr.20170707]

5   **Yabuuchi H**, Fukuya T, Tajima T, Hachitanda Y, Tomita K, Koga M. Salivary gland tumors: Diagnostic value of gadolinium-enhanced dynamic MR imaging with histopathologic correlation. *Radiology* 2003; **226**: 345-354 [PMID: 12563124 DOI: 10.1148/radiol.2262011486]

6   **Lechner Goyault J**, Riehm S, Neuville A, Gentine A, Veillon F. Interest of diffusion-weighted and gadolinium-enhanced dynamic MR sequences for the diagnosis of parotid gland tumors. *J Neuroradiol* 2011; **38**: 77-89 [PMID: 20542568 DOI: 10.1016/j.neurad.2009.10.005]

7   **Abdel Razek AA**, Samir S, Ashmalla GA. Characterization of Parotid Tumors With Dynamic Susceptibility Contrast Perfusion-Weighted Magnetic Resonance Imaging and Diffusion-Weighted MR Imaging. *J Comput Assist Tomogr* 2017; **41**: 131-136 [PMID: 27636248 DOI: 10.1097/RCT.0000000000000486]

8   **Yuan Y**, Tang W, Tao X. Parotid gland lesions: Separate and combined diagnostic value of conventional MRI, diffusion-weighted imaging and dynamic contrast-enhanced MRI. *Br J Radiol* 2016; **89**: 20150912 [PMID: 26892378 DOI: 10.1259/bjr.20150912]

9   **Mikaszewski B**, Markiet K, Smugała A, Stodulski D, Szurowska E, Stankiewicz C. Diffusion- and Perfusion-Weighted Magnetic Resonance Imaging-An Alternative to Fine Needle Biopsy or Only an Adjunct Test in Preoperative Differential Diagnostics of Malignant and Benign Parotid Tumors? *J Oral Maxillofac Surg* 2017; **75**: 2248-2253 [PMID: 28412261 DOI: 10.1016/j.joms.2017.03.018]

10 **Yabuuchi H**, Matsuo Y, Kamitani T, Setoguchi T, Okafuji T, Soeda H, Sakai S, Hatakenaka M, Nakashima T, Oda Y, Honda H. Parotid gland tumors: Can addition of diffusion-weighted MR imaging to dynamic contrast-enhanced MR imaging improve diagnostic accuracy in characterization? *Radiology* 2008; **249**: 909-916 [PMID: 18941162 DOI:

10.1148/radiol.2493072045]

11 **Gökçe E**, Beyhan M. Advanced magnetic resonance imaging findings in salivary gland tumors. *World J Radiol* 2022; **14**: 256-271 [PMID: 36160835 DOI: 10.4329/wjr.v14.i8.256]

12 **Eida S**, Sumi M, Nakamura T. Multiparametric magnetic resonance imaging for the differentiation between benign and malignant salivary gland tumors. *J Magn Reson Imaging* 2010; **31**: 673-679 [PMID: 20187211 DOI: 10.1002/jmri.22091]

13 **Munhoz L**, Ramos EADA, Im DC, Hisatomi M, Yanagi Y, Asaumi J, Arita ES. Application of diffusion-weighted magnetic resonance imaging in the diagnosis of salivary gland diseases: A systematic review. *Oral Surg Oral Med Oral Pathol Oral Radiol* 2019; **128**: 280-310 [PMID: 31029591 DOI: 10.1016/j.oooo.2019.02.020]

14 **Yabuuchi H**, Kamitani T, Sagiyama K, Yamasaki Y, Hida T, Matsuura Y, Hino T, Murayama Y, Yasumatsu R, Yamamoto H. Characterization of parotid gland tumors: Added value of permeability MR imaging to DWI and DCE-MRI. *Eur Radiol* 2020; **30**: 6402-6412 [PMID: 32613285 DOI: 10.1007/s00330-020-07004-3]

15 **Huang N**, Xiao Z, Chen Y, She D, Guo W, Yang X, Chen Q, Cao D, Chen T. Quantitative dynamic contrast-enhanced MRI and readout segmentation of long variable echo-trains diffusion-weighted imaging in differentiating parotid gland tumors. *Neuroradiology* 2021; **63**: 1709-1719 [PMID: 34241661 DOI: 10.1007/s00234-021-02758-z]

16 **Tofts PS**, Brix G, Buckley DL, Evelhoch JL, Henderson E, Knopp MV, Larsson HB, Lee TY, Mayr NA, Parker GJ, Port RE, Taylor J, Weisskoff RM. Estimating kinetic parameters from dynamic contrast-enhanced T(1)-weighted MRI of a diffusable tracer: Standardized quantities and symbols. *J Magn Reson Imaging* 1999; **10**: 223-232 [PMID: 10508281 DOI: 10.1002/(sici)1522-2586(199909)10:3<223::aid-jmri2>3.0.co;2-s]

17 **Celebi I**, Mahmutoglu AS, Ucgul A, Ulusay SM, Basak T, Basak M. Quantitative diffusion-weighted magnetic resonance imaging in the evaluation of parotid gland masses: A study with histopathological correlation. *Clin Imaging* 2013; **37**: 232-238 [PMID: 23465973 DOI: 10.1016/j.clinimag.2012.04.025]

18 **Assili S**, Fathi Kazerooni A, Aghaghazvini L, Saligheh Rad HR, Pirayesh Islamian J. Dynamic Contrast Magnetic Resonance Imaging (DCE-MRI) and Diffusion Weighted MR Imaging (DWI) for Differentiation between Benign and Malignant Salivary Gland Tumors. *J Biomed Phys Eng* 2015; **5**: 157-168 [PMID: 26688794]

19 **Milad P**, Elbegiermy M, Shokry T, Mahmoud H, Kamal I, Taha MS, Keriakos N. The added value of pretreatment DW MRI in characterization of salivary glands pathologies. *Am J Otolaryngol* 2017; **38**: 13-20 [PMID: 27806890 DOI: 10.1016/j.amjoto.2016.09.002]

20 **Tao X**, Yang G, Wang P, Wu Y, Zhu W, Shi H, Gong X, Gao W, Yu Q. The value of combining conventional, diffusion-weighted and dynamic contrast-enhanced MR imaging for the diagnosis of parotid gland tumours. *Dentomaxillofac Radiol* 2017; **46**: 20160434 [PMID: 28299943 DOI: 10.1259/dmfr.20160434]

21 **Eida S**, Sumi M, Sakihama N, Takahashi H, Nakamura T. Apparent diffusion coefficient mapping of salivary gland tumors: Prediction of the benignancy and malignancy. *AJNR Am J Neuroradiol* 2007; **28**: 116-121 [PMID: 17213436]

22 **Elmokadem AH**, Abdel Khalek AM, Abdel Wahab RM, Tharwat N, Gaballa GM, Elata MA, Amer T. Diagnostic Accuracy of Multiparametric Magnetic Resonance Imaging for Differentiation Between Parotid Neoplasms. *Can Assoc Radiol J* 2019; **70**: 264-272 [PMID: 30922790 DOI: 10.1016/j.carj.2018.10.010]

23 **Habermann CR**, Arndt C, Graessner J, Diestel L, Petersen KU, Reitmeier F, Ussmueller JO, Adam G, Jaehne M. Diffusion-weighted echo-planar MR imaging of primary parotid gland tumors: Is a prediction of different histologic subtypes possible? *AJNR Am J Neuroradiol* 2009; **30**: 591-596 [PMID: 19131405 DOI: 10.3174/ajnr.A1412]

24 **Faheem MH**, Shady S, Refaat MM. Role of magnetic resonance imaging (MRI) including diffusion weighted images (DWIs) in assessment of parotid gland masses with histopathological correlation. *Egypt J Radiol Nucl Med* 2018; **49**: 368-373 [DOI: 10.1016/j.ejrnm.2018.03.001]

25 **Ogawa T**, Kojima I, Ishii R, Sakamoto M, Murata T, Suzuki T, Kato K, Nakanome A, Ohkoshi A, Ishida E, Kakehata S, Shiga K, Katori Y. Clinical utility of dynamic-enhanced MRI in salivary gland tumors: Retrospective study and literature review. *Eur Arch Otorhinolaryngol* 2018; **275**: 1613-1621 [PMID: 29623392 DOI: 10.1007/s00405-018-4965-9]

26 **Lam PD**, Kuribayashi A, Imaizumi A, Sakamoto J, Sumi Y, Yoshino N, Kurabayashi T. Differentiating benign and malignant salivary gland tumours: Diagnostic criteria and the accuracy of dynamic contrast-enhanced MRI with high temporal resolution. *Br J Radiol* 2015; **88**: 20140685 [PMID: 25791568 DOI: 10.1259/bjr.20140685]

27 **Abdel Razek AAK**, Mukherji SK. State-of-the-Art Imaging of Salivary Gland Tumors. *Neuroimaging Clin N Am* 2018; **28**: 303-317 [PMID: 29622121 DOI: 10.1016/j.nic.2018.01.009]

28 **Huang N**, Chen Y, She D, Xing Z, Chen T, Cao D. Diffusion kurtosis imaging and dynamic contrast-enhanced MRI for the differentiation of parotid gland tumors. *Eur Radiol* 2022; **32**: 2748-2759 [PMID: 34642805 DOI: 10.1007/s00330-021-08312-y]